DOI:10.15918/j.jbit1004-0579.2008.01.008
Journal of Beijing Institute of Technology, 2008, Vol. 17, No. 1

Three-Dimensional Simulation of Plasma Jet and Particle Groups in Plasma Spraying

FAN Qun-bo(范群波), WANG Lu(王鲁), WANG Fu-chi (王富耻)
(School of Material Science and Engineering, Beijing Institute of Technology, Beijing 100081, China)

Abstract: The temperature field, velocity field, as well as species distribution in three-dimensional space are successfully calculated by establishing three-dimensional geometry model and solving plasma jet-substrate interaction equations, optimized particle trajecory models, as well as particle-particle heat transfer equations in three-dimensionalal space. Under typical working conditions, the flying trajectories and distribution of ZrO_2 ceramic particles and Ni metal particles are also simulated. Results show that, the plasma jet becomes wider near the substrate, and the stochastic trajectory model is preferable to simulate the turbulent diffusion effect of particles. In addition, Ni metal particles penetrate relatively more deeply than ZrO_2 ceramic particles due to larger density.

Key words: three-dimensional simulation; plasma jet; particles
CLC number: TG 374 **Document code**: A **Article ID**: 1004-0579(2008)01-0115-07

It has been widely accepted that two-dimension geometrical model is available to solve plasma-particle momentum and mass transportation problems. From the very first stage when Eckert and Pfender et al[1] provided a comprehensive introduction to plasma heat transfer to the later moment when Lee[2] and Mckelliget[3] began to investigate the interaction between the plasma jet and the particles, most investigations are limited to two-dimension model, including some recent studies carried out by Nylen[4] and Nishiyama[5]. When we discuss the particle spatial distribution and further the deposition process on the substrate, however, a three-dimensional (3D) model must be used[6].

Therefore, in recent years more and more people begin to employ a 3D model to investigate plasma jet, which is more similar to real conditions. Dussoubs[7] calculated a 3D plasma jet without particles by solving an optimization turbulence model. In his later work[8], both 2D and 3D models coupled with metal and ceramic particles are proposed. However, a more comprehensive study is still necessary. In the present work, the three-dimensionalal temperature and velocity fields, the spatial distribution of species and particles are calculated. Some important 3-D information, such as the three-dimensionalal continuous isothermal lines, isovelocity lines, and the 3-D appearance of the plasma jet and particle groups are described, which is hard to be obtained with a 2-D scheme.

1 Mathematical Model

The model is based on the following assumptions:

① The plasma is in local thermodynamic equilibrium, which is composed of two spicies: primary gas argon (Ar) and secondary gas helium (He).

② Since ionization energy of He is far higher than that of Ar, and there is little He^{+} below 10 000 ℃, we only consider the ionization reaction of argon, $Ar^{+} + e \longleftrightarrow Ar$.

③ The particles injected into the plasma jet are regarded as ideal smooth spheres.

Received 2006-12-08
Sponsored by the Ministerial Level Foundation (A12050914); the Excellent Young Teacher Foundation of Beijing Institute of Technology (1040012040101)
Biography FAN Qun-bo(1974—), lecturer, Ph. D., fanqunbo@bit.edu.cn.

④ Knudsen effect and solid state phase transitions among the particles are negligible.

⑤ The plasma jet flow is a steady-state system.

1.1 Equations of the Interaction Between the Plasma Jet and the Substrate

The interaction between the high-velocity plasma jet and the substrate surface can be described by the wall function[9], which may be written as

$$\frac{U'}{u_*}=2.5\ln\frac{du_*}{\nu}+b, \qquad (1)$$

where U' is the tangential velocity at a distance d from the wall; $u_*=\sqrt{\tau_s/\rho}$ is the shear speed, and τ_s is the wall shear stress; ν is the molecular kinematical viscosity; b is a constant equal to 5.5[10], which depends on the wall roughness.

The heat transfer from the plasma to the substrate can be expressed as

$$q=h_f(T_s-T_f), \qquad (2)$$

where q is the heat flux from the plasma jet to the target; h_f is the heat transfer coefficient; T_s is the temperature on the substrate surface; T_f is the temperature of the plasma jet.

1.2 Particle Trajectory Models

To predict the trajectories of flying particles, Crowe[11] proposed to calculate the motion of the plasma jet in the Euler coordinate system, while particle motion in the Lagrange coordinate system. During the computational analysis, the plasma jet without particles shall be calculated at the very first stage till a coarse convergence. Then, on the basis of the plasma jet, the particle velocity, trajectory, and temperature are calculated and all the particle results are substituted into the equations involved in solving the plasma jet, until all the mathematical procedures are converged. We call this methodology "general Lagrange model". Although general Lagrange model takes into account the complex coupling effects of the plasma jet and particle groups, it neglects the turbulent diffusion effects of particles.

With respect to motions of particle groups in practical thermal spraying, there is both slip motion component of time averaged velocity along the particle trajectories and diffusion motion component interspersing between two sides of the particle trajectories. Affected by particle material type, particle size, feed rate of powders, as well as many other factors, particles are randomly dispersed in three-dimensional space. Therefore, a stochastic trajectory model shall be introduced.

In this paper, two different trajectory models are employed and compared. The turbulent diffusion effect is taken into account in the introduced stochastic trajectory models[12], assuming that when particles are in the plasma vortex, the stochastic fluctuation velocity of the gas unit volume keeps a constant; once the vortex escapes, a new stochastic velocity will be generated. The particle velocity can therefore be

$$v_p=f(v_g, v_g', \tau_p), \qquad (3)$$

where v_g is the mean velocity of the plasma gas; v_g' is the stochastic fluctuation velocity, and τ_p is the particle relaxation time.

If the particle is in the plasma vortex, then

$$v_g=\eta\sqrt{\overline{v}_g'}, \qquad (4)$$

where $\sqrt{\overline{v}_g'}$ is the mean square root of the plasma gas turbulent fluctuation velocity; η is a stochastic number fitting normal distribution. During the vortex life cycle, η keeps a constant.

By means of integrating particle instantaneous velocity, particle flying trajectories can be obtained.

1.3 Plasma-Particle Heat Transfer Equations

The plasma-particle heat transfer equation can be written as

$$m_p c_p\frac{dT_p}{dt}=hA_p(T_\infty-T_p)+\varepsilon_p A_p\sigma(T_a^4-T_p^4), \qquad (5)$$

where m_p, c_p, T_∞, T_p and h are particle mass, particle specific heat, plasma temperature, particle temperature, and convective heat transfer coefficient, respectively; ε_p the particle irradiation rate; σ the Boltzmann constant, and T_a the ambient temperature.

There is also heat transfer inside the particle. For a ideal spherical particle, the heat transfer equation inside the particle can be represented as

$$\frac{\partial H}{\partial t}=\frac{1}{r^2}\frac{\partial}{\partial r}\left(k_p r^2\frac{\partial T}{\partial r}\right), \qquad (6)$$

where r is the radial coordinate; H and k_p are particle enthalpy and thermal conductivity, respectively; T is the temperature.

1.4 Geometry and Boundary Conditions

The geometrical model shown in Fig. 1a is defined as a cylindrical 3-D domain, which consists of 26693 elements. In the radial direction, the grid is more refined near the central axis and coarser towards the outer environment. Fig. 1b shows the meshed vertical section and the computational sizes. The nozzle diameter of the plasma gun is 8 mm, and the target stands 80 mm away from the jet. As illustrated in Fig. 1b, the powder port is located axially 8.0 mm downstream from the nozzle exit and vertically 13 mm above the axis of the nozzle.

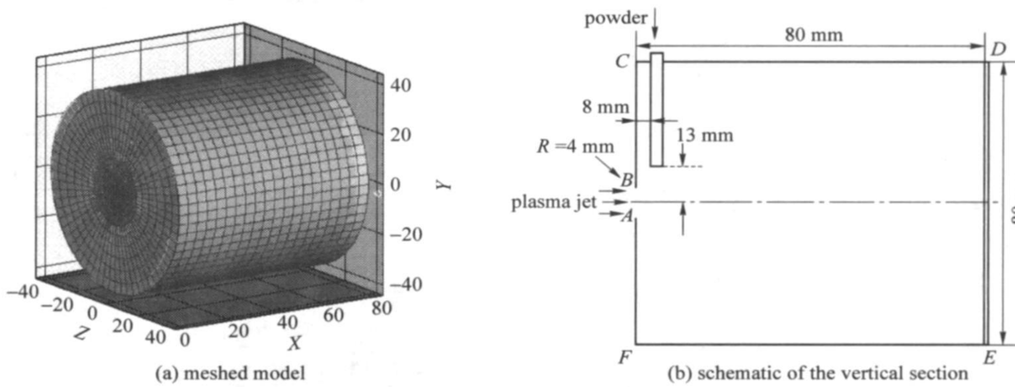

Fig. 1 Geometrical model for the 3D computational domain

Boundary conditions, such as dynamic and thermodynamic conditions like turbulent intensity, characteristic length, temperature, pressure, as well as species mole fractions, at the places AB, BC, CD, EF, FA, and DE can be given according to Ref.[13] published by the author.

2 Results and Discussion

Fig. 2 shows the simulated 3D contours of temperature and velocity under typical operation conditions (I = 900 A, F_{Ar} = 70 scf/h, F_{He} = 30 scf/h) in free plasma jet or when the substrate is not considered.

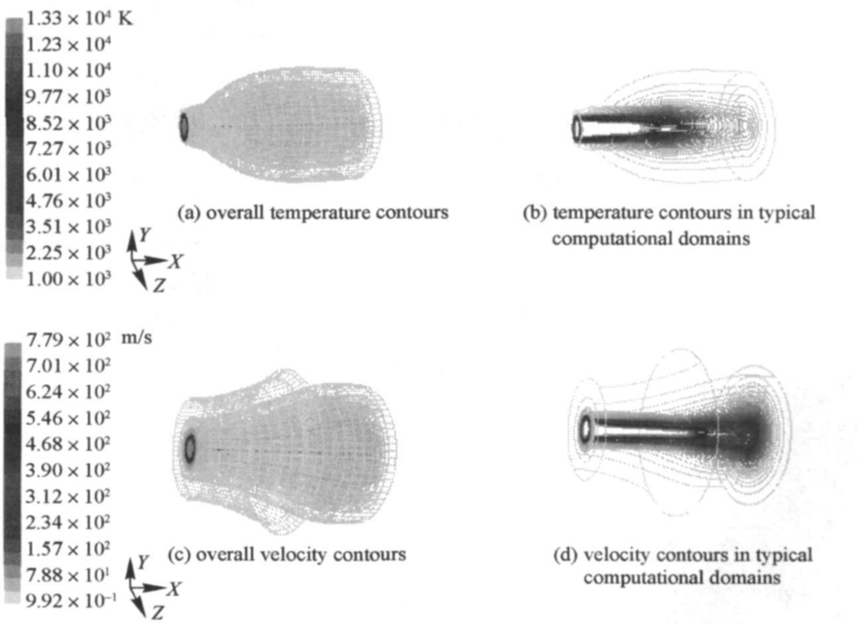

Fig. 2 Three dimensional temperature field without substrate

Fig. 2a presents the overall temperature contours, and Fig. 2b shows temperature contours in typical computational domains, including the vertical section, inlet plane and outlet plane of the plasma jet field. Fig. 2c and Fig. 2d show the overall velocity contours and velocity contours in the same field as in Fig. 2b, respectively. The intervals of the isothermal and isovelocity lines shown in Fig. 2 are 1 200 K and 80 m/s, respectively.

It can be seen from Fig. 2 that the temperature and velocity at the plasma core don't change significantly, since the ambient air doesn't penetrate into this zone. But at 80 mm away from the nozzle exit, the corresponding temperature decreases to 1 000 K, and the velocity decreases to 260 m/s. At a certain axial distance, the temperature and velocity along the radial direction also decrease due to strong heat and momentum transfer in plasma spraying. It might be noted that while the air is entrained into the computational domain, the width of the plasma jet becomes wider with the increase of the axial distance.

Fig. 3 and Fig. 4 show the 3D spatial distribution of Ar atom mass fraction contours and He atom mass fraction contours in the overall field and in the typical computational domains, with 9% Ar and 0.4% He atom concentration interval, respectively. Fig. 3 and Fig. 4 illustrate that the corresponding Ar and He mass fractions decrease sharply to 0 at the outlet of the plasma jet filed. And at a fixed axial distance, the mass fractions along the radial direction also drop. The mass diffusion mechanism is similar to that in the heat diffusion and presents a tendency from non-equilibrium to equilibrium.

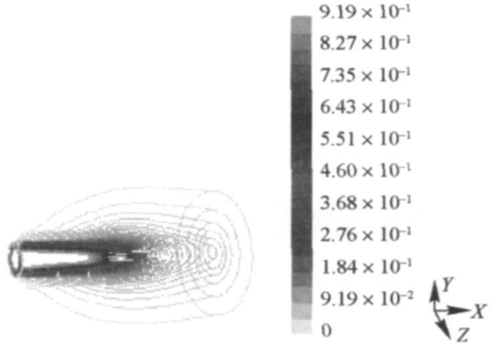

Fig. 3 Spatial distribution of Ar atom concentration contours in 3D plasma jet without substrate

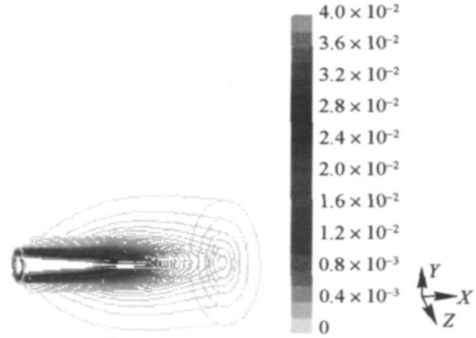

Fig. 4 Spatial distribution of He atom concentration contours in 3D plasma jet without substrate

Fig. 5 shows the simulated 3D contours of temperature and velocity under typical operation conditions ($I = 900$ A, $F_{Ar} = 70$ scf/h, $F_{He} = 30$ scf/h) when the substrate is taken into account. Fig. 5a presents the overall temperature contours, and Fig. 5b shows the temperature contours in the typical computational domains, including the vertical section, inlet plane and outlet plane of the plasma jet field. The intervals of the isothermal lines shown in Fig. 5a and Fig. 5b are 1 200 K. Fig. 5c and Fig. 5d show the overall velocity contours and the velocity contours in the typical domains with the interval of 80 m/s, respectively.

It can be seen from Fig. 3 and Fig. 5 that if the substrate is considered in the numerical simulation procedures, the plasma jet would interact with not only the ambient air but also the substrate, exchanging heat and momentum. The plasma jet becomes more wider and appears to be a "cone hat" due to the interaction between the plasma and the substrate. Under the predefined boundary conditions, at 80 mm away from the nozzle exit, the corresponding temperature decreases to 1 000 K, while the velocity decreases sharply to 0. At a certain axial distance, the temperature and velocity values along the radial direction also decrease. The difference resulted from the existence of the substrate will definitely affect the heating of the particles and particle trajectories. However, at the plasma core or around this zone, there is not an obvious difference. The temperature or the velocity even fits a similar descending tendency at the position

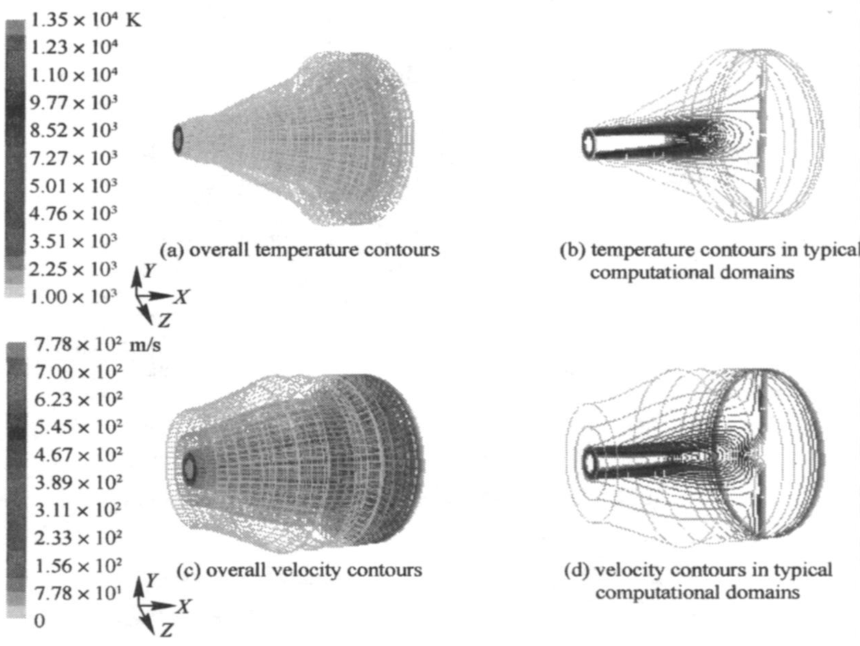

Fig. 5 Three dimensional temperature field with substrate

far from the substrate.

Fig.6 and Fig.7 show the 3D spatial distribution of Ar atom mass fraction contours and He atom mass fraction contours in the overall field and in the typical computational domains, with 9% Ar atom contour interval and 0.4% He atom contour interval, respectively. Compared with Fig.3 and Fig.4, except near the substrate where the species span an obviously wider range, the concentration distribution presents a similar diffusion tendency if without the substrate. When the plasma jet is far from the plasma core, the concentration of the two species approaches to 0, indicating that the mass transfer between the plasma jet and the ambient air has gradually ended.

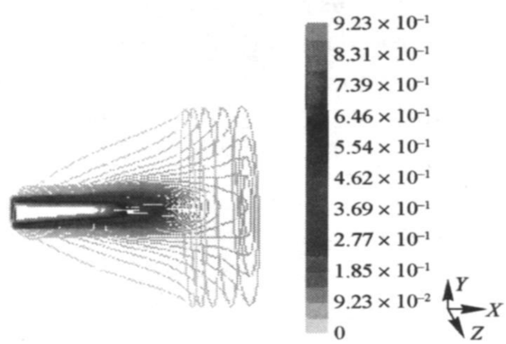

Fig. 6 Spatial distribution of Ar atom concentration contours in 3D plasma jet with substrate

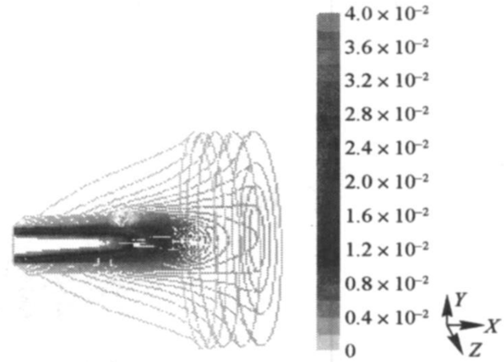

Fig. 7 Spatial distribution of He atom concentration contours in 3D plasma jet with substrate

Fig. 8 shows the particle trajectories of 10 ZrO_2 particles and 10 Ni particles with diameters of 45—80 μm by using general Lagrange model. Fig.8a presents the particle trajectories, and Fig.8b shows the corresponding particle distribution on the substrate. It can be seen that if the turbulent diffusion effect is not taken into account, particles would move strictly along their trajectories and limited in the *XY* plane without any mutual inference. As illustrated in Fig.8b, Ni particles penetrate more deeply into the plasma jet than ZrO_2 particles due to metal nickel's larger density. Therefore, in plasma spraying if powders of two different materials are sprayed simultaneously, they would not overlap each other completely.

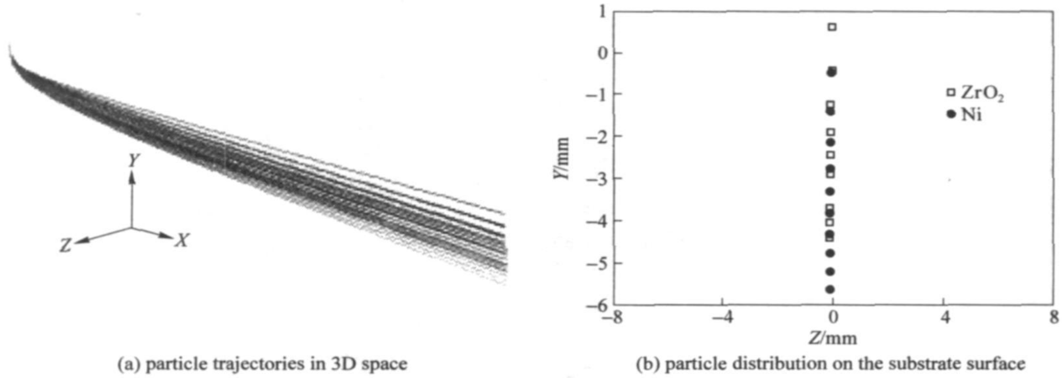

Fig. 8 Particle trajectories calculated by traditional Lagrange trajectory model

Fig. 9 shows the particle trajectories of 100 ZrO_2 particles and 100 Ni particles with diameters of 45—80 μm by employing stochastic trajectory model. Fig. 9a presents the particle trajectories and Fig. 9b shows the corresponding particle disperse distribution on the substrate. It can be seen that the turbulent fluctuation of the plasma jet makes so significant effect on the particle trajectories that particles distribute randomly and stochastically in the 3D space, instead of limited in the *XY* plane. As a matter of fact, in practical plasma spraying, basic turbulence parameters such as fluctuation frequency, amplitude, as well as direction, would affect the particle trajectories. Therefore, the 3D stochastic trajectory model is a preferable model in numerical simulation.

Although particles in 3D space and on the substrate distribute randomly, we can still see that Ni particles penetrate more deeply into the plasma jet due to relatively larger density, and the two particle groups of different materials don't overlap each other completely. When spraying functionally gradient materials (FGM), the particle groups of different materials shall overlap each other as much as possible to get a uniform coating with steady properties. Therefore, two methods are proposed: one way is to inject two types of particles through two separate injectors and the positions of the two injectors shall be adjusted so as to control the particle flying trajectories; the other way is to spray two types of particles through a single injector and the particle trajectories can be controlled by adjust the particle diameters. Based on the particle disperse distribution on the substrate, the corresponding 3D appearance and the 2D species distribution of the FGM coating can be further predicted[14].

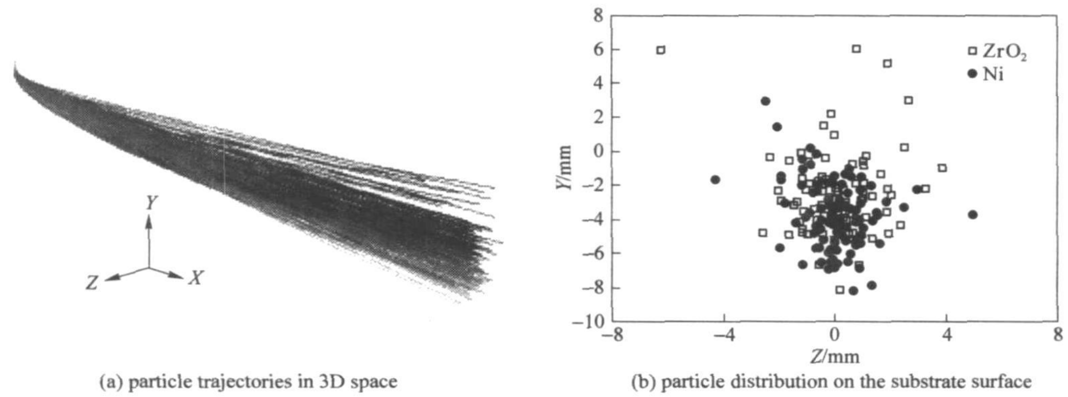

Fig. 9 Particle trajectories calculated by stochastic trajectory model

3 Conclusions

In this paper, a three-dimensional geometry model and corresponding mathematical models are employed to calculate the 3D temperature field, velocity field and species spatial distribution under typical operation conditions. The effect of substrate existence on the calculated results is investigated. In addition, the particle trajectories simulated by employing two different particle trajectory models are compared and discussed. With respect to functionally gradient materials, the particle distributions of two different materials in 3D space and on the substrate are analyzed.

① By introducing wall function and plasma-substrate heat transfer equations, the interaction between the plasma jet and the substrate is calculated. It is found that the spanning of the plasma jet near the substrate becomes wider and the velocity of the plasma jet approaches to zero. In other areas, however, the temperature field, velocity field, as well as species distribution, are similar to free plasma jet (without substrate).

② If employing common Lagrange trajectory model, the particle trajectory will be limited strictly in a plane; if a stochastic turbulent model is employed, the stochastic particles dispersion in three-dimensional space and on the substrate can be simulated, which nearly approaches to real conditions.

③ Under the same operational conditions, Ni particles will penetrate more deeply into the plasma jet than ZrO_2 particles due to nickel's relatively larger density, indicating that when spray functionally gradient coatings, the particle groups of two different materials would not well overlap each other, but can be adjusted through some technique methods.

References:

[1] Eckert E R G, Pfender E. Advances in plasma heat transfer [M]. New York: Academic Press, 1967.

[2] Lee Yungcheng. Modeling work in thermal plasma process [D]. Minnesota: University of Minnesota, 1984.

[3] EL-Kaddah N, Mckelliget J, Szekely J. Heat transfer and fluid flow in plasma spraying [J]. Metallurgical Transcactions B, 1984, 15B(1): 59—70.

[4] Nylen P, Wigren J, Pejryd L, et al. The modeling of coating thickness, heat transfer, and fluid flow and its correlation with the thermal barrier coating microstructure for a plasma spayed gas turbine application [J]. Journal of Thermal Spray Technology, 1999, 8(3): 393—398.

[5] Nishiyama H, Kuzuhara M, Solonenko O P, et al. Numerical modeling of an impinging dusted plasma jet controlled by a magnetic field in a low pressure [C] //Thermal Spray: Meeting the Challenges of the 21st Century. Nice, France: ASM International, 1998: 451—456.

[6] Fauchais P, Vardelle A. Heat, mass and momentum transfer in coating formation by plasma spraying [J]. International Journal of Thermal Sciences, 2000, 39(9): 852—870.

[7] Dussoubs B, Fauchais P, Vardelle A, et al. Computational analysis of a three-dimensional plasma spray jet [C] //Thermal Spray: A United Forum for Scientific and Technological Advances. Indianapolis: ASM International, 1997: 557—565.

[8] Dussoubs B, Vardelle A, Mariaux G, et al. Modeling of plasma spraying of two powders [J]. Journal of Thermal Spray Technology, 2001, 10(1): 105—110.

[9] Amsden A A, Ramshaw J D, O'Rourke P J, et al. KIVA: A computer program for two and three-dimensionalal fluid flows with chemical reactions and fuel sprays [R]. Los Alamos: Los Alamos National Laboratory Report, 1985.

[10] Chang C H. Numerical simulation of Alumina spraying in an Argon-Helium jet [C] //Proceedings of the International Thermal Spray Conference & Exposition. Orlando: ASM International, 1992: 793—798.

[11] Crowe C T, Elger D F, Roberson J A. Engineering fluid mechanics [M]. 7th ed. Boston: John Wiley & Sons, 2000.

[12] Chen Kefa, Fan Jianren. Theory and calculation of industrial gas and solid multi-phase fluid [M]. Hangzhou: Press of Zhejiang University, 1990. (in Chinese)

[13] Fan Qunbo, Wang Lu, Wang Fuchi. Numerical simulation of basic parameters in plasma spray [J]. Transactions of Beijing Institute of Technology, 2004, 13(1): 80—84.

[14] Wang Lu, Fan Qunbo, Wang Fuchi, et al. Numerical simulation of plasma-sprayed functionally graded coatings [C] //Proceedings of the International Thermal Spray Conference. Osaka, Japan: ASM International, 2004: 806—811.

(**Editor**: Cai Jianying)